Soft Matter

PAPER

Dynamic properties of different liquid states in systems with competing interactions studied with lysozyme solutions†

Cite this: DOI: 10.1039/c8sm01678j

P. D. Godfrin, *[ab] P. Falus,[c] L. Porcar,[c] K. Hong,[d] S. D. Hudson,[e] N. J. Wagner[b] and Y. Liu*[bf]

Recent studies of colloidal systems with a short-range attraction and long-range repulsion (SALR) have been demonstrated to have a generalized phase diagram with multiple liquid states defined by their structures. In this paper, we identify the different liquid states of previous experimentally studied lysozyme samples within this proposed generalized state diagram and explore the dynamic properties of each liquid state. We show that most lysozyme samples studied here and previously at low and intermediate concentrations are dispersed fluids while a few high concentration samples are randomly percolated liquids. In the dispersed fluid region, the short-time diffusion coefficient measured by neutron spin echo agrees well with the long time diffusion coefficient estimated with the solution viscosity. This dynamic feature is maintained even for some samples in the random percolated region. However, the short-time and long-time diffusion coefficients of random percolated fluids deviate at larger concentration and attraction strength. At high enough concentrations, the mean square displacement can be as slow as those of many glassy colloidal systems at time scales near the characteristic diffusion time even though these lysozyme samples remain in liquid states at the long-time limit. We thus identify the region in the generalized phase diagram where these equilibrium states with extremely slow local dynamics exist relative to bulk percolation and kinetic arrest (gel and glassy) transitions.

Received 15th August 2018,
Accepted 2nd October 2018

DOI: 10.1039/c8sm01678j

rsc.li/soft-matter-journal

Introduction

Dynamic and structural properties of protein solutions have long been studied due to their importance for many biological systems and industrial applications such as protein crystallization and pharmaceutical formulation.[1] Despite the complexity of protein surface properties and protein–protein interactions, it has been shown that interactions between many globular proteins can be reasonably approximated by isotropic interaction potentials. For solutions of many globular proteins in the presence of large salt concentrations, the thermodynamics can be accurately calculated and predicted based on a short-ranged attraction, such as shown for lysozyme.[1–5] In solutions with very low ionic strength, many globular proteins can be accurately represented by a combination of a short-ranged attraction and a long-ranged electrostatic repulsion (SALR).[6–8] Over the past decade, there has been increased research interest in SALR colloidal systems, particularly the conditions of kinetic arrest, in part due to the importance of protein solutions and for identifying a fundamental physical description of gel and glass formation.

The gelation and glass transitions of SALR systems have been widely studied experimentally using large colloidal particles suspended in organic solvent that can be visualized by confocal microscopy. The formation of Bernal spiral clusters in gel states has been observed by experiments and computer simulations,[4,5] as well as several other non-equilibrium states.[9] In comparison, the study of protein solutions with a SALR interaction has been mostly focused on liquid states.

[a] Department of Chemical Engineering, Massachusetts Institute of Technology, Cambridge, MA 02139, USA
[b] Center for Neutron Science, Department of Chemical and Biomolecular Engineering, University of Delaware, Newark, DE 19716, USA. E-mail: godfrin@udel.edu, yunliu@udel.edu
[c] Institut Laue-Langevin, 38042 Grenoble Cedex 9, France
[d] Center for Nanophase Materials and Sciences, Oak Ridge National Laboratory, Oak Ridge, TN 37831, USA
[e] Polymers and Complex Fluids Group, National Institute of Standards and Technology, Gaithersburg, MD 20899, USA
[f] Center for Neutron Research, National Institute of Standards and Technology, Gaithersburg, MD 20899, USA. E-mail: yunliu@nist.gov

† Electronic supplementary information (ESI) available: Details pertaining to the SANS data, the MC simulation methods and the cluster distribution calculated therein, and calculations of the characteristic diffusion time are provided. See DOI: 10.1039/c8sm01678j

Interestingly, it has been shown that the short-time dynamics are closely related with dynamic cluster formation for many protein solutions,[10–12] which is important for understanding the viscosity behaviour at elevated concentrations, such as in monoclonal antibody formulations.[13,14] By systematically studying the short time dynamics and the rheological properties of lysozyme protein solutions at low salt conditions, it has been shown that the normalized short time dynamics at high concentrations can be as slow as the dynamics of many colloidal systems in glassy states despite the fact that the studied lysozyme samples remain in liquid states.[15] The formation of intermediate range order (IRO) has been shown to be the driving force for this slow dynamics.[15] It is worth pointing out that the formation of IRO, driven by the competition of the short-range attraction and long-range repulsion, is one of the hallmark structural features of SALR systems. IRO can be experimentally determined by observing a scattering peak in the inter-particle structure factor at a wave vector much smaller than that of the nearest neighbour scattering peak. Interestingly, the hydrodynamic function also shows the IRO peak,[16,17] which is supported by the results from experiment, theoretical calculations, and computer simulations.[18,19] These findings are consistent with other theories that couple the static and dynamic properties of concentrated systems.[20,21]

The competition between a short-ranged attraction and a long-ranged repulsion produces a very diverse landscape of equilibrium and non-equilibrium states.[9] Several simulation studies have identified a variety of equilibrium and kinetically arrested states by simulation and experimentation. A recent simulation effort has classified different equilibrium liquid states in SALR systems and established a generalized state diagram by relating several of these liquid states (*e.g.*, dispersed fluid state, random percolated state, clustered fluid state, cluster percolated state) to purely attractive phase behavior.[22] However, the dynamic properties of these liquid states within this generalized state diagram have not been experimentally investigated, leaving many questions regarding the effect(s) of dynamics on macroscopic properties, such as viscosity. Therefore, it is very interesting to investigate experimental samples to locate the phase space of liquid states and understand their dynamic and macroscopic properties. In this paper, we use lysozyme as a model system to first identify the liquid states of several previously studied samples, and then examine the diffusivity and viscosity of samples within each region of the generalized phase diagram for SALR systems. These results will thus provide fundamental physical insights into the properties of SALR systems.

Experimental and theoretical methods

Sample preparation

Lysozyme was obtained from MP Biomedicals and subsequently purified to remove excess counter-ions to maintain the lowest ionic strength possible. The as received lysozyme was purified by dialyzing against deionized water at around 4 °C until the resistance of the water reached around 18.0 M ohm (typically about 48 hours, by seven changes of deionized water) and then lyophilized by using freeze drying. Samples were prepared at room temperature by resuspending lyophilized purified protein in deuterium oxide and filtered through 0.22 μm filters. Use of D_2O has minimal effects on solution behaviour, but avoids the large incoherent scattering background of water for the neutron scattering experiments. Samples above 300 mg mL^{-1} were prepared at 50 °C to expedite the dissolution process and subsequently filtered with 0.45 μm filters due to their high viscosity. The highest concentration samples showed signs of crystallization after roughly 12 hours, but remained stable over the time scale of all experiments.

Small angle neutron scattering experiments and analysis

Small angle neutron scattering was performed on the D-33 beamline at Institut Laue-Langevin (ILL) in Grenoble, France and the NG-7 SANS at the NIST Center for Neutron Research (NCNR) in Gaithersburg, MD. The raw data at NCNR was reduced using NCNR software.[23] SANS data of lysozyme solutions are modelled as mono-dispersed spherical particles resulting in $I(q) = \phi V(\Delta\rho)^2 P(q)S(q) + B$, where ϕ is the volume fraction determined from the skeleton density of lysozyme,[24] V is the volume of a particle, $(\Delta\rho)^2$ is the neutron scattering length density difference between particles and solvent, B is the background, and $P(q)$ and $S(q)$ are the form factor and effective structure factor, respectively. Due to hydrogen–deuterium exchange between the deuterated solvent and labile hydrogens in the protein, the solvent–protein scattering contrast is a function of protein concentration and is used as an additional fitting parameter (see the ESI†). An integral equation theory (IET) consisting of a thermodynamically self-consistent closure relation with the Ornstein–Zernike equation was used to fit $S(q)$ and extract interaction parameters.[25] The potential used for these calculations was the hard sphere double Yukawa potential

$$\frac{U_{\mathrm{HSDY}}(r)}{kT} = \begin{cases} \infty & r < 1 \\ \left(-K_1 e^{-z_1(r-1)} + K_2 e^{-z_2(r-1)}\right) & r \geq 1 \end{cases}, \quad (1)$$

where r is the reduced protein–protein separation normalized by the particle diameter, σ, z_1 and z_2 are the inverse ranges of attraction and repulsion, respectively, and K_1 and K_2 are the strengths of attraction and repulsion, respectively, relative to thermal energy. The attraction range was fixed at 10% of the protein diameter based on the method proposed before[8] and the long-ranged repulsion was constrained by the generalized one component model of electrostatic repulsion.[26]

Neutron spin echo experiments and analysis

Neutron spin echo experiments were performed on the IN-15 beamline at the ILL. Seven instrument configurations were used to obtain the intermediate scattering function, $S(q,t)$, with a Fourier time up to 50 ns over a range of q-values from 0.04 $Å^{-1}$ to 0.2 $Å^{-1}$. In general, the intermediate scattering function of macromolecules measured by NSE is complicated and the

This journal is © The Royal Society of Chemistry 2018

dynamic decoupling approximation can be used to explain the data over the full q range.[27] The collective diffusion coefficient, $D_c(q)$, is quantified by fitting $S(q,t)$ over a correlation time less than the characteristic time of diffusion, t_D, with an exponential decay function. t_D is defined as $t_D = 3\pi\eta_S\sigma^3/4k_BT$, where k_BT is the thermal energy, and η_S is the solvent viscosity (t_D values for lysozyme are shown in the ESI†). The self-diffusion coefficient, D_s, can be obtained from the asymptotic high-q limit of $D_c(q)$. In our experiment, it was taken as the average value between 0.1 Å^{-1} and 0.16 Å^{-1}. Although in this q-range $S(q) \neq 1$, the q-dependence of the structure factor, $S(q)$, and hydrodynamic function, $H(q)$, compensate each other,[19] which allows the short-time self-diffusion coefficient to be quantified from the diffusion coefficient at the intermediate q-range used here. For values of $q\sigma/2 > 1$, it has been shown that $S(q,t)$ can be reduced to the self-intermediate scattering function even at very high concentrations.[28] Hence, the mean squared displacement can be calculated from $S(q,t)$ according to $\langle R^2\rangle = -[6/q^2]\ln[S(q,t)]$. The MSD is calculated as the average of the functions obtained from the intermediate scattering functions at q-values between 0.1 Å^{-1} and 0.16 Å^{-1}. The MSDs are normalized by the particle diameter, $\langle R^{*2}\rangle = \langle R^2\rangle/\sigma^2$, as a function of dimensionless time, $t^* = t/t_D$.

Simulation details

Solution structures are calculated and visualized by running Metropolis Monte Carlo (MC) simulations of 1728 particles in the *NVT* ensemble with periodic boundary conditions. All particles have pair wise interactions defined by the HSDY interaction potential with parameters extracted from fits to the SANS data. Starting from a simple cubic lattice, each system is thermalized for 2×10^7 steps. After equilibration, thermodynamic and structural parameters were averaged over 4×10^4 independent configurations. The initial displacement distance of 0.1σ is dynamically adjusted to maintain an acceptance ratio of 30%. Calculations of solution structure factors are completed following previously defined protocols.[22,29] Connectivity is defined as a particle being within a distance equal to the zero energy point of the potential.[22,30] Percolation in these systems is defined as having 50% of sampled configurations containing a system spanning cluster.[31]

Results and discussion

SALR systems can have a wide variety of liquid states, as identified by simulation[22] and experimental[9] studies. To determine the liquid states of the lysozyme samples previously studied, we need to obtain the interaction potential between lysozyme proteins for samples at different conditions. We used SANS to study the interaction potential between lysozyme proteins in solution. Note that the final results of interaction potentials of lysozyme samples were reported briefly in the ESI† of our previous papers.[15,19] Here, for the completeness of the discussion, we first provide the missing details in the previous papers about the experimental procedure and the analysis method together with the simulation results to verify our analysis method.

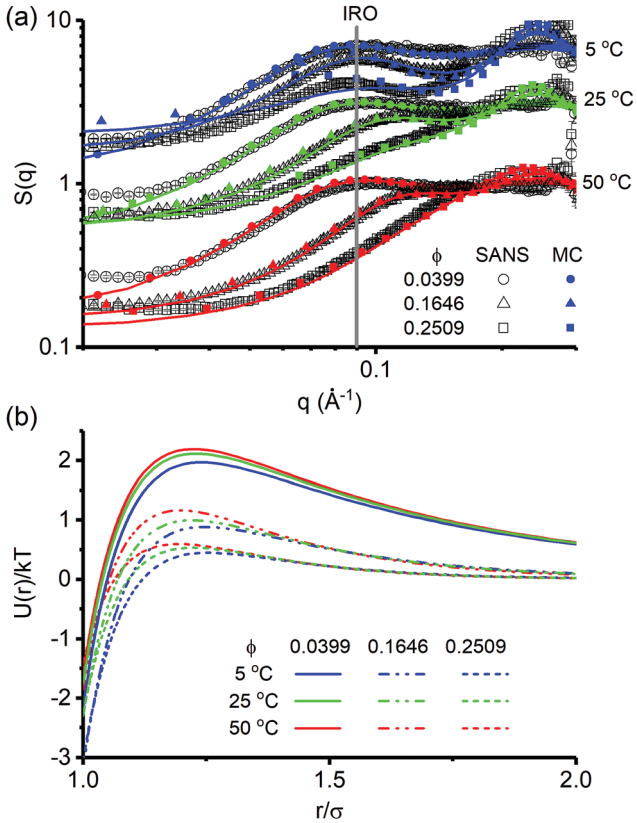

Fig. 1 (a) Inter-particle structure factors obtained from normalizing SANS data (black, open symbols, replotted from a prior publications[15,19]) with best fits using IET (lines, replotted from a prior study[19]) and calculations from MC simulations (colored, filled symbols). All data points at 5 °C and 25 °C are shifted vertically for clarity. The solid grey line marks the q-value of IRO peak formation. (b) The interaction potentials extracted from IET fits to the SANS data shown in (a) are plotted together.

The SANS data of the investigated lysozyme samples, prepared as discussed in the Methods section, span concentrations from 10 to 480 mg mL^{-1} at temperatures ranging from 5 °C to 50 °C. Shown in Fig. 1a are the inter-protein structure factors $S(q)$, extracted from the experimental coherent scattering intensity, $I(q)$. (Data at different temperatures are shifted vertically.) The most prominent feature of $S(q)$ is the formation of a low-q peak, or IRO peak, at low temperatures that is consistently found at roughly 0.09 Å^{-1} for many of the solution conditions. Long-ranged electrostatic repulsion maintains a homogeneous solution structure over large length scales, reflected in the suppressed $S(q)$ magnitude at small q-values, while short-ranged attraction drives association over shorter length scales. These competing forces are what drive IRO formation.

Inter-protein interactions can be quantified through the analysis of $S(q)$,[25] which can be accurately described with an SALR interaction under the low ionic strength conditions of these samples. The coherent scattering intensity of SANS can be described as $I(q) = AP(q)S(q)$ for a monodispersed, spherical

particle system. As shown in the ESI,† the normalized intensities for all concentrations and temperatures overlap at high q-values, which probe the length scale of individual proteins, indicating that the globular structure of lysozyme is maintained under all solution conditions. Therefore, variations in the q-dependence of $I(q)$ at low q-values are related to changes in inter-protein interactions. It is well known that decreasing the temperature increases the attraction strength between lysozyme proteins so that the inter-protein structure factor, $S(q)$, is strongly temperature dependent.

The magnitude and range of the interaction potential at different sample conditions is extracted from fits to $S(q)$ using IET for systems with the hard sphere double-Yukawa (HSDY) potential,[25] where one Yukawa term is used to simulate the short-ranged attraction and another Yukawa term is used to simulate the long-ranged electrostatic repulsion.[32,33] The fits to the experimental $S(q)$ are shown as solid lines in Fig. 1a, which converged for all temperatures. The interaction potentials shown in Fig. 1b are the results extracted from the fits to the data in Fig. 1a, plotted as a function of the center to center distance normalized by the protein diameter. As the protein concentration increases, the counter-ion concentration also increases, causing the strength and range of repulsion to decrease. The extracted HSDY potentials also show a monotonic increase in the strength of attraction with decreasing temperature.[1] During the fitting, the volume fraction of the protein is one of the fitting parameters and determines the real volume fraction of protein in solution, ϕ_{fit}. Values of ϕ_{fit} from the SANS fitting can be compared to the volume fraction calculated from the skeleton density, ϕ. As shown in Table 1, ϕ_{fit} and ϕ are almost identical. For $\phi > 0.30$, the fitting algorithm does not converge and could not fit the data likely due to the limitations of the algorithm used here. It is important to note that these lysozyme samples are at equilibrium states, which the use of IET methods requires. However, achieving convergence and thermodynamic self-consistency will require a closer examination of the computer algorithm.

The IET method has been implemented and validated with Monte Carlo (MC) simulations for lysozyme samples previously.[19] Fig. 1a demonstrates the good agreement between the $S(q)$ from experiment (open symbols) and that calculated from the MC simulations (solid symbols), and the IET theory (solid lines), which provides confidence in the extracted interaction potentials as well as the additional structural properties extracted from MC simulations.

With the lysozyme interaction potential obtained by fitting SANS data, the state points of all lysozyme samples in the generalized phase diagram can be determined for the first time. Note that even though there have been a few papers that studied concentrated lysozyme protein solutions by SANS/SAXS, the type of liquid states as SALR systems have never been reported before for lysozyme samples. Placing state points of protein solutions on a generalized state diagram[22] requires that the Baxter parameter, τ_{B}, is estimated from the reference attractive potential. The reference attractive potential, $V_{\mathrm{Ref}}(r)$, is defined as the attractive portion of the full SALR potential based on the previous report using computer simulations.[22] Using the reference attractive potential obtained from the fitting, the second virial coefficient can be estimated as $B_{2,\mathrm{ref}} = -2\pi\int_0^{r_c}\left(\mathrm{e}^{-\frac{V_{\mathrm{Ref}}(r)}{k_{\mathrm{B}}T}}-1\right)r^2\mathrm{d}r$, where r_c is the cut off distance. From the previous results, r_c is chosen as the separation distance at which the total SALR potential crosses zero. The normalized second virial coefficient, $B_{2,\mathrm{ref}}^*$, is thus defined as the ratio between $B_{2,\mathrm{ref}}$ and the second virial coefficient of a hard sphere system. Thus, The calculation of τ_{B} is defined as $\tau_{\mathrm{B}} = 1/4(B_2^* - 1)$. In a SALR system, τ_{B} is thus only determined by the attractive part of the total SALR potential. The generalized phase diagram proposed previously shows that if the range of the attraction is small enough, the details of the potential shape of the short range attraction does not matter.[22]

Table 1 shows τ_{B} for samples over the full range of protein concentrations and temperatures studied. It is noted that for $0.10 < \phi < 0.3$, τ_{B} does not change much when increasing the concentration. This is clearer when plotting τ_{B} as a function of ϕ (solid symbols) shown in Fig. 2. Therefore, it is reasonable to speculate that for samples at even higher concentrations, τ_{B} would not change too much. Hence, for $\phi > 0.30$, τ_{B} was approximately estimated as the average value of the four points for the volume fraction between 0.1 and 0.3.

With known values of τ_{B} and ϕ, all experimental state points (solid circles) are then placed in the generalized phase diagram proposed recently and shown in Fig. 2. (Note that the state points for $\phi > 0.30$ are distinguished as open symbols.) For context, the binodal line (gray solid line) and glass lines (gray dashed lines) for the reference attractive hard sphere (AHS) system are also included.[34] Based on the previously proposed generalized phase diagram of the SALR system, the region above the binodal line of the reference AHS system has two different types of states that are separated by the percolation line of the SALR system. The state points on the left of the percolation line are in the dispersed fluid state, while the state points on the right of the percolation line are in the random percolated state. Lastly, the glass transition lines are based on mode coupling theory (MCT) calculations with the widely used shift in volume fraction to account for the under-prediction of the experimentally observed glass transition by the theory.

Table 1 Summary of protein volume fractions and Baxter parameters (replotted from a prior study[15]) extracted from fits to the SANS data for each sample protein concentration and temperature studied. Under conditions where the IET fitting could not converge (italicized), τ_{B} values are estimated as an average of the previous four states and ϕ_{fit} is assumed to be equal to ϕ

Temp.	5 °C		25 °C		50 °C	
ϕ	ϕ_{fit}	τ_{B}	ϕ_{fit}	τ_{B}	ϕ_{fit}	τ_{B}
0.0399	0.040	0.763	0.040	1.348	0.040	1.742
0.0800	0.077	0.245	0.077	1.087	0.074	2.774
0.1215	0.126	0.190	0.129	0.499	0.126	1.263
0.1646	0.143	0.192	0.147	0.503	0.155	0.956
0.2070	0.202	0.167	0.210	0.395	0.209	1.289
0.2509	0.239	0.184	0.240	0.428	0.244	1.328
0.2981		*0.183*		*0.457*		*1.209*
0.3448		*0.183*		*0.457*		*1.209*

This journal is © The Royal Society of Chemistry 2018

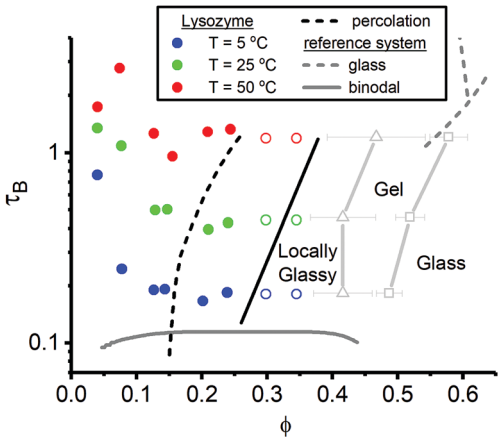

Fig. 2 An effective state diagram of lysozyme is produced in which state points with an SALR potential are plotted relative to the AHS binodal and glass lines (gray solid and dashed lines, respectively)[34] as well as the SALR percolation line (black dashed line). With increasing volume fraction, the samples transition from a dispersed fluid to a dynamically percolated state (across the percolation line) and subsequently to a locally glassy state (across the solid black line). At higher volume fractions, gel and glass transitions for SALR systems (light gray symbols and lines) are estimated from power law extrapolations of viscosity and NSE data, respectively.

The percolation transition of our experimental lysozyme samples is estimated by our MC simulations (see the ESI†). However, given the limited solution conditions that are experimentally available, we will compare our state points to previous MC simulations covering a larger range of concentrations with similar competing interactions.[35] The percolation line (black short dashed line) in Fig. 2 is replotted from this more detailed simulation study using an SALR potential with parameters that closely mimic those of the lysozyme samples studies here (*i.e.*, a relative strength of repulsion to attraction of 1.0 and a range of repulsion of 0.65σ). For our lysozyme samples, the relative strength of repulsion to attraction remains roughly 0.7, while the range of repulsion shifts from 0.83σ at low concentration to 0.33σ at high concentration. Therefore, the lower strength and longer range found in lysozyme samples compensate each other, yielding a calculated percolation transition that quantitatively corresponds to our states (shown in the ESI†) shown in Fig. 2.

Most of the lysozyme samples are in the dispersed fluid state of the generalized phase diagram. For higher concentrations, some of the samples are in the random percolated state. As defined in previous work,[22] dispersed fluids are equilibrium states consisting of a polydisperse distribution of monomers and clusters and random percolated states contain a system spanning network. Since all the state points are above the binodal line of the reference AHS system, none of the lysozyme samples have clusters with an optimal size even though some of them show a strong, clear IRO peak in $S(q)$, as shown in Fig. 1a.

Having identified the type of liquid states for different lysozyme samples, their dynamic features and macroscopic properties can be compared. The short-time diffusion coefficient, D_s, obtained from the NSE is plotted in Fig. 3a relative to calculations for hard sphere systems.[36] NSE measures $D_c(q)$ at a wide range of q values, from which D_s is determined. Based on the dynamic decoupling approximation, the self-translational

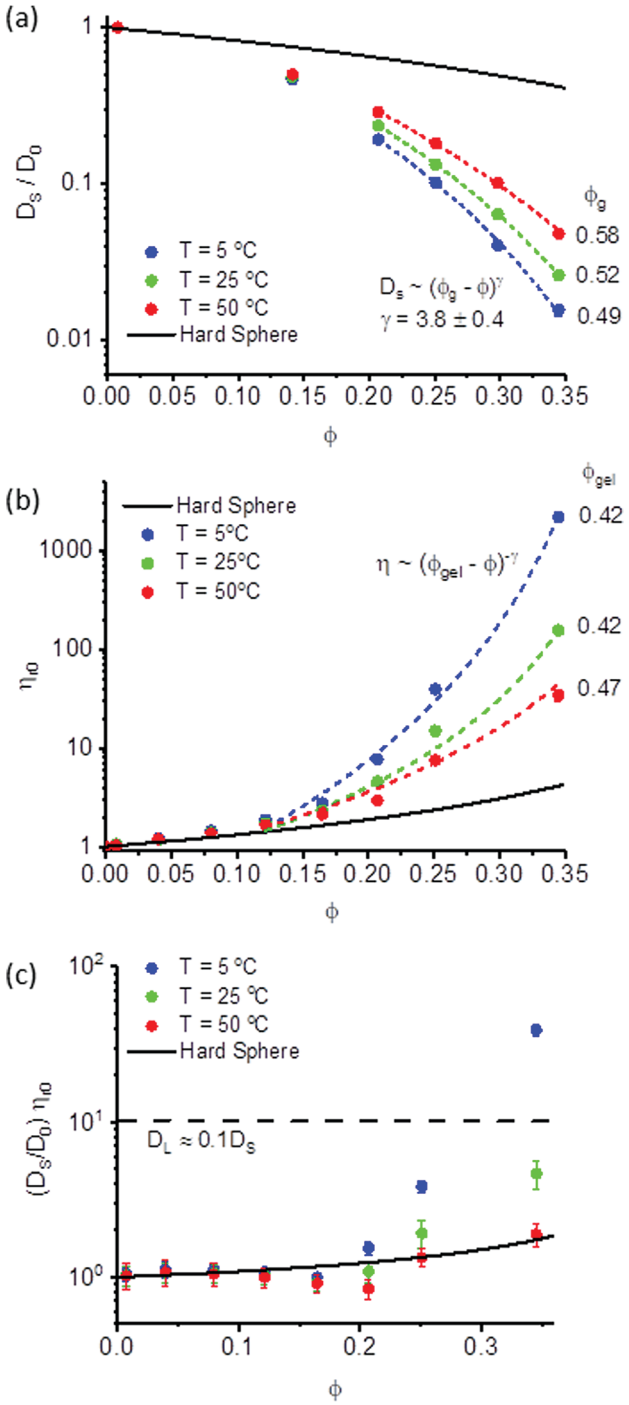

Fig. 3 The (a) normalized short-time self diffusion coefficients and (b) reduced zero shear viscosity of lysozyme are plotted relative to the volume fraction dependence of hard sphere systems[36,40] (solid line). Viscosity data in (b) are replotted form an earlier publication.[15] The colored dotted lines in (a and b) are fits to extrapolate glass and gel transitions, respectively. (c) A plot of the ratio of short-time dynamics to the effective long-time dynamics (represented by the inverse of η_{r0}) of lysozyme (symbols) relative to hard sphere expectations (solid line). The most viscous sample surpasses the Löwen freezing criteria[41] (dashed line) originally proposed for hard sphere systems.

motions can be obtained at relatively high-q.[27] Thus the mean square displacement can be extracted at different q values at the short time limit ($t < t_D$) following the method discussed in the Experimental and theoretical methods section, from which the short-time diffusion coefficient can be determined. The self-diffusion coefficients shown in Fig. 3a are estimated by averaging the asymptotic value at large q-values with $q > 0.1$ Å^{-1}.

At lower temperatures, the short-time self-diffusion coefficient decreases particularly quickly as a function of volume fraction due to stronger attractive interactions. For $\phi < 0.16$, the normalized diffusion coefficient, D_s/D_0, is not sensitive to the temperature change (from 50 °C to 5 °C), despite a decrease in τ_B from a value of between 1 and 3 to a value close to 0.1. Note that when $\phi < 0.16$, all the lysozyme samples studied here are all in the dispersed fluid region. Therefore, particles in dispersed fluids can be considered as freely diffusive in the short time limit with little influence from the short-range attraction strength. This result is consistent with a previous study showing that at about 10% mass fraction lysozyme dispersed in heavy water, there is little temperature dependence of the normalized diffusion coefficient over a very wide range of temperature.[12]

However, many computer simulations including our own, show that dispersed fluid states contain many clusters that are sensitively dependent on the strength of the short-range attraction. By increasing the attraction strength, the average cluster size increases. These simulation results seem to contradict with our experimental observation as the increased average cluster size is expected to slow down the short time diffusion coefficient. Here, we would like to clarify that computer simulations determine whether two particles are bound together purely based on the distance between two particles. If the distance between particles is smaller than a certain cut off distance, these two particles are claimed to be in the same cluster. We term these type of clusters based on the geometric configuration as geometrically connected clusters. On the other hand, NSE probes the cluster formation by measuring the ensemble averaged diffusion coefficient. Therefore, the definition of clusters investigated by NSE is intrinsically different from geometrically connected clusters. The fact that the short-time diffusion coefficient at the dispersed fluid region is not affected too much by the attraction strength indicates that most geometrically connected clusters investigated by computer simulations are loosely bounded (or transient)[10] clusters. However, cluster formation and therefore diffusivity is still a strong function of volume fraction, as shown in Fig. 3a.

Interestingly, for $\phi > 0.16$, most lysozyme samples are in the randomly percolated region. At these volume fractions, the normalized short-time diffusion coefficient is very sensitive to the temperature, which means that it is very sensitive to the change of the short-range attraction. Note that in the randomly percolated state, most particles in a system are in a percolated cluster. We again reiterate that the percolated cluster is one type of geometrically connected cluster. When many geometrically connected clusters exist in a randomly percolated state, the chance to have strongly bounded clusters increases by increasing attraction strength. Therefore, the short-time diffusion coefficient decreases. Of course, if the attraction strength keeps increasing, the strongly bounded clusters can grow much bigger so that NSE can only probe the local motions due to the crowded environment in large clusters. The transition from loosely bounded clusters to systems having a significant amount of strongly bounded clusters can be slow and smooth, which is reflected by the change of the normalized short-time diffusion coefficient as a function of concentration. This slow transition is in stark contrast to purely attractive systems that rapidly develop an elastic modulus above the percolation transition due to rigidity percolation.[37,38] As we will discuss in more detail later, the gradual reduction in diffusivity reflects the distribution of local environments (*i.e.*, local densities) in which individual particles find themselves.

Similar smooth transitions in the colloidal dynamics of SALR systems have been observed by the evolution of a "gel plateau" in the intermediate scattering function when simultaneously increasing attraction and repulsion strength.[5] In contrast, increasing bond lifetime at constant attraction strength leaves local relaxation unaffected, but extends the timescale of alpha (or cage) relaxation, τ_α, at volume fractions approaching a gel or glass transition.[39] Thus, short-time relaxation is dictated by short-range attraction, which is consistent with the temperature dependence of our NSE data. However, unlike these prior experimental and simulation studies, NSE is unable to probe timescales beyond roughly $4\tau_D$, where τ_D is the characteristic diffusion time. Therefore, we are unable to directly detect a gel plateau if one exists.

In addition to short-time dynamics, we quantify the long-time dynamics by measuring solution viscosity, which is a good approximation of the inverse of the long-time diffusion coefficient. Prior work has demonstrated that values of τ_α for a colloidal gel can be as long as $10^7\tau_D$. Here, rheological measurements of lysozyme are capable of probing timescales of roughly $10^9\tau_D$, which far exceed the observation time frame of any other experimental or simulation system studied to date. Thus, we are capable of truly observing the long-time state of this SALR system.

The viscosity behaviour of lysozyme samples in both dispersed fluid states and randomly percolated fluid states have been measured with a microcapillary viscometer. Interestingly, the results in Fig. 3b (plotted relative to hard sphere calculations[40]) show that for $\phi \leq 0.16$, the relative viscosity is also temperature insensitive when the temperature changes between 5 °C and 50 °C. This implies that changing τ_B in the dispersed fluid region will not significantly shift the relative viscosity. Therefore, the long-time dynamics in a dispersed fluid state are not very sensitive to the change of the attraction in a SALR system. However, when $\phi > 0.16$, most samples are in the random percolated fluid region. The relative viscosity becomes very sensitive to the temperature. Only two high concentration samples are in the dispersed fluid region at high temperatures (50 °C), which can transition to a random percolated fluid by decreasing the temperature to 25 °C or lower. The

 This journal is © The Royal Society of Chemistry 2018

key structural feature of random percolated fluids is the formation of randomly percolated clusters. Thus, the temperature–sensitive relative viscosity change observed at high lysozyme concentration is attributed to the percolation. As expected, given a fixed τ_B, increasing the concentration will increase the viscosity. Also, the viscosity is expected to be very sensitive to τ_B in the random percolated fluid region. This is experimentally observed in the random percolated fluids studied here, as their viscosity increases much faster as a function of concentration than dispersed fluid states.

Despite the dramatic increase in viscosity, all samples flow as Newtonian liquids under shear. Even though there is a dramatic decrease in short-time diffusivity, it is unclear whether a non-ergodic plateau evolves in the intermediate scattering function at high volume fractions (due to the limited time window of NSE). Interestingly, Löwen *et al.* showed that dynamic arrest of hard sphere and attractive colloidal suspensions is well correlated with the reduction of long-time diffusion below 10% of the short-time diffusion.[41] It is thus very interesting to understand the relative change of short and long time diffusion coefficients in a SALR system and compare it with the Löwen criterion.

In Fig. 3c, the product of the normalized short-time diffusion coefficient and the relative zero-shear viscosity is plotted as a function of lysozyme volume fraction compared to hard sphere estimates. This product is essentially the ratio between the short-time and long-time diffusion coefficient, D_s/D_L. Hard sphere calculations remain near a value of one until they diverge at volume fractions approaching the glass transition (not shown in Fig. 3c). However, for our lysozyme solutions at lower temperatures, this ratio deviates significantly from a value of one at elevated volume fractions but with much smaller volume fraction than that of hard sphere systems with similar ratios of D_s/D_L. In fact, the ratio D_s/D_L of the most viscous sample actually surpasses the Löwen criterion for freezing even though the lysozyme solution remains as a liquid state with a volume fraction of about 34%. Given the finite viscosity and short-time diffusivity of this lysozyme sample, the Löwen criterion does not imply macroscopic arrest in our systems, but may serve as a useful indicator of locally hindered dynamics.

Our prior work demonstrated that the normalized MSDs, measured by NSE, of some lysozyme solutions at very high concentrations are slower than many colloidal systems in glass states despite having a finite viscosity and diffusivity. This dynamic behaviour was termed as a localized glassy behaviour. As discussed in the previous work,[15] these glassy like dynamics result from the onset of intermediate range order caused by SALR interactions. By comparing the MSDs of lysozyme samples to the MSDs of micrometer sized particles measured with a confocal microscope, a few lysozyme samples are identified as in this localized glassy state. Now, having quantified the interaction potentials, these localized glassy states can be located in the generalized phase diagram.

The transition to a localized glassy state region is demarcated by a solid black line in Fig. 3, and is well inside the random percolated region. (Note that only three samples were identified to be in the localized glassy states. Therefore, the boundary cannot be identified very accurately.) When the volume fraction is just slightly over the percolation transition, proteins remain mobile at both local and macroscopic scales. By further increasing the protein concentration, the absolute magnitudes of the MSDs quickly decrease and eventually are below that of previously reported locally glassy behavior in systems with competing interactions over the full range of time scales studied.

We reiterate that NSE is unable to probe timescales long enough to observe the presence of a gel or non-ergodic plateau, if one exists. Given the uniquely short characteristic diffusion time of lysozyme, it is possible that the highest volume fraction samples experimentally studied have characteristic features of gelled states yet have sufficient time to structurally relax over relevant timescales of observation. Therefore, future work is necessary to determine if these locally glassy states are a distinct state with unique dynamics or are true gels. Quantifying lysozyme dynamics (*i.e.*, MSDs and intermediate scattering functions) over intermediate timescales is the focus of ongoing simulation, but for now remain uncertain.

Given that gels are also defined as the onset of a yield stress under an applied shear, a gel transition volume fraction is estimated by fitting the viscosity data with a power law function similar to previous work.[11] The power law representation is used to extract a volume fraction at which divergence is expected to occur according to $\eta_0 = A(\phi_{gel} - \phi)^{-\gamma}$, where A is a constant, γ is the exponent, and ϕ_{gel} is the gel point. The fits are shown in Fig. 3b as dotted lines along with labels of the extracted gelation volume fraction and the extracted parameters are summarized in the ESI.† These values are also plotted on the state diagram in Fig. 2. The true presence of the estimated gel region is uncertain, since it remains unknown whether lysozyme samples will display either a non-ergodic plateau or a yield stress at these elevated volume fractions. Note that gelation is intimately connected with the observation timescale. While prior studies have quantified gelation by observation of a non-ergodic plateau, this approach is infeasible with lysozyme given the limitations of instrumental resolution. However, previous studies varying bonding time and/or strength demonstrate that the gel transition depends intimately on the strength and range of repulsion as well as the observation timescale relative to the diffusive timescale.[4,5,39] Additionally, the mean squared displacement of many systems considered as gels have increasing magnitudes even at the longest timescales probed, suggesting incomplete relaxation.[5,42] Thus, these studies may have observed relaxation if their observation timescale were extended.

Interestingly, the estimated volume fraction for the gel transition using our viscosity data agrees surprisingly well with the maximum local density (*i.e.*, the primary peak value) observed in gelled states. The local density, ϕ_L, represents the volume fraction of neighboring particles around a reference particle as a function of separation distance. It is quantified similar to previous studies[4,25] by integration of the radial

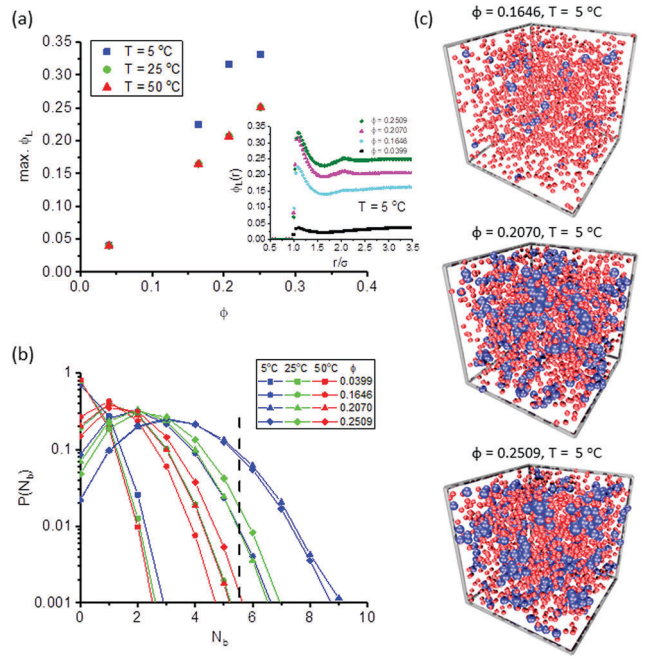

Fig. 4 (a) The maximum local density is plotted as a function of bulk volume fraction for each temperature studied. The inset shows the radial density distribution for each state studied at 5 °C. (b) The nearest neighbour distribution is plotted for each solution condition reproduced by MC simulation. Some of the data are replotted from a previous publication.[19] (c) Characteristic configurations are provided for four state points of lysozyme suspensions generated by MC simulations using the potentials extracted from SANS. Particles in clusters are shown in red and those with six or more neighbors are shown in blue (monomers are not shown for clarity).

distribution function according to

$$\phi_L(r) = \frac{3\phi}{r^3}\int_0^r x^2 g(x)\mathrm{d}x. \quad (2)$$

It is largely driven by attraction, and was previously identified to be also around 0.4 in colloidal gels for disparate ranges of repulsion.[4,22,39] Simulations show that the long-time dynamics are very sensitive to the repulsive component of the interaction potential only at solution conditions above this volume fraction (see Fig. 9 in ref. 39). The consistency of ϕ_L suggests that this volume fraction may represent an energetically favourable packing in SALR gels. Further, it is physically intuitive that this local volume fraction might serve as an upper limit to bulk gelation.

In Fig. 4, values of ϕ_L extracted from our MC simulations show that lysozyme samples at 5 °C are approaching the consistent gel value of 0.4 at volume fractions around 0.3. That the most dynamically hindered locally glassy state studied here (ϕ = 0.35, T = 5 °C) surpasses the Löwen criterion for freezing (see Fig. 3c)[41] suggests that this state point may in fact be at least very close to a gelled state.

The onset of non-ergodicity in colloidal systems has also been associated with the prevalence of particles with at least six neighbors.[43,44] Therefore, in the absence of NSE at long timescales, Fig. 4 provides a measure of the nearest neighbour distribution (extracted from the radial distribution function of MC simulations). Fig. 4 also shows configuration snapshots from MC simulations of four state points studied, where particles having at least six nearest neighbors are highlighted in blue. For the samples with sub-diffusive behaviour over short times, the local structure of these states are found to have an increased content of particles in crowded environments (six or more neighbors).[5] As protein volume fraction increases further and short-ranged attraction becomes stronger, the relative fraction of proteins in these locally crowded environments is expected to increase. Correspondingly, more widespread collective rearrangement is necessary to escape these regions, leading to the locally-glassy behaviour observed by NSE.

In comparison with colloidal systems with only a short-ranged attraction, the local structure of lysozyme samples inside the locally glassy region is similar to a gel sample, as both show strong heterogeneous density distributions. However, the long-ranged repulsions keep the heterogeneous density localized to the length scale comparable to the intermediate range order. The density distribution remains relatively uniform at large length scales. This special structural feature may therefore serve as the source of some special dynamic features. As shown in a previous simulation study of SALR systems,[5] the dynamics of systems with a strong IRO peak show that the longest relaxation times occur over IRO lengthscales when approaching the gel transition. Further, recent work combining theory, experiment, and simulation demonstrate that hydrodynamic contributions to structural relaxation is strongest over IRO lengthscales as quantified by a peak in the hydrodynamic function at the same q-value as found in the structure factor.[19] These lengthscale dependent dynamics have been observed in prior work, but described in terms of two distinct populations, namely slow and fast particles, rather than structural properties.[45]

By further increasing protein concentration, a true glass transition may eventually occur. As an estimate of the glass transition, the volume fraction dependence of D_s is also fit with a power law function (as done previously)[46] identical to that used for η_0 but with a positive exponent and ϕ_{gel} replaced with ϕ_g (the estimated glass transition point), while requiring the same exponent for all temperatures (shown as dotted lines in Fig. 3a). The fitted values of ϕ_g (summarized in the ESI†) quantifies where self-diffusivity approaches zero. The glass transition defined by MCT does not dictate that D_s = 0, but the extracted value of ϕ_g *via* that assumption will closely resemble the volume fraction at which a glassy state is formed (where a non-ergodic plateau forms in the MSD) due to the rapidly decreasing (finite) value of short-time diffusivity as a function of ϕ.[46] The extracted glass transition is also plotted on the state diagram in Fig. 2. Interestingly, our estimated glass line approaches that of an AHS system at large τ_B values and volume fractions. The apparent ability to distinguish percolation, gel, and glass transitions in SALR systems is distinctly different from prior work using purely attractive systems where percolation and gelation are found to occur under identical solution conditions.[37] It is worth noting that gel and glass transitions have several characteristic features than may be used in their identification,[47] and thus alternative

This journal is © The Royal Society of Chemistry 2018

measurements may cause quantitative deviations to the transitions reported here, but the qualitative differences in macroscopic (gel) and microscopic (glass) kinetic arrest should be maintained across techniques/definitions. Thus, these samples provide both preliminary evidence on the unique behaviour of SALR systems and further understanding of the general features of kinetic arrest. Future studies will be aimed at further refining the conditions of locally-glassy dynamics and the influence of competing interactions on the bulk gel and glass transitions.

Conclusions

To summarize, the interaction potential between lysozyme solutions was quantified and used to identify the different types of liquid states proposed recently. It is found that most lysozyme samples studied here and in previous papers are in either the dispersed fluid states or randomly percolated states. In the dispersed fluid states, both the short-time behaviour, measured by NSE, and the long-time behavior, studied by measuring the zero shear viscosity, are nearly independent of the short-range attraction strength, similar to previous reports.[19] This indicates that the clusters formed in the dispersed fluid state are loosely bounded clusters. Further, the ratio of the short-time and long-time diffusion coefficient is estimated. In the dispersed fluid region, the short and long time diffusion coefficient is almost the same. Therefore, the dynamics of the systems in the dispersed fluid region are dominated by monomer particles. On the contrary, both the short and long time dynamics of samples in the randomly percolated fluid state are very sensitive to the change of the short-range attraction. Additionally, the short and long time diffusion coefficients deviate from each other. This decoupling of dynamics at different time scales indicates that the effects of clustering in the randomly percolated fluid region play a significant role in material properties. Lastly, the region in which the local dynamics are as slow as those of many colloidal systems in glass states while rheological measurements display Newtonian behaviour was identified as the localized glass state. This region of the state diagram precedes estimates of gelation and glass transitions determined by extrapolating measurements of rheology and short time dynamics, respectively. This behaviour is seemingly unique to SALR systems but may also help clarify the general behavior of kinetic arrest in colloidal systems, and therefore prompts further study.

Conflicts of interest

There are no conflicts to declare.

Acknowledgements

This manuscript was prepared under cooperative agreements 70NANB12H239 and 70NANB10H256 from NIST, U.S. Department of Commerce. Certain commercial equipment, instruments, or materials are identified in this document. Such identification does not imply recommendation or endorsement by the National Institute of Standards and Technology nor does it imply that the products identified are necessarily the best available for the purpose. Y. L. acknowledges the support by the Center for High Resolution Neutron Scattering (CHRNS), a partnership between the National Institute of Standards and Technology and National Science Foundation under Agreement No. DMR-1508249.

References

1 A. C. Dumetz, A. M. Chockla, E. W. Kaler and A. M. Lenhoff, *Biophys. J.*, 2008, **94**, 570–583.
2 D. Rosenbaum, P. Zamora and C. Zukoski, *Phys. Rev. Lett.*, 1996, **76**, 150–153.
3 N. E. Valadez-Pérez, A. L. Benavides, E. Schöll-Paschinger and R. Castañeda-Priego, *J. Chem. Phys.*, 2012, **137**, 084905.
4 A. Campbell, V. Anderson, J. S. van Duijneveldt and P. Bartlett, *Phys. Rev. Lett.*, 2005, **94**, 208301.
5 F. Sciortino, P. Tartaglia and E. Zaccarelli, *J. Phys. Chem. B*, 2005, **109**, 21942.
6 Y. Liu, E. Fratini, P. Baglioni, W.-R. Chen and S.-H. Chen, *Phys. Rev. Lett.*, 2005, **95**, 2–5.
7 A. Stradner, F. Cardinaux and P. Schurtenberger, *J. Phys. Chem. B*, 2006, **110**, 21222–21231.
8 Y. Liu, L. Porcar, J. Chen, W. Chen, P. Falus, A. Faraone, E. Fratini, K. Hong and P. Baglioni, *J. Phys. Chem. B*, 2011, **115**, 7238–7247.
9 C. L. Klix, C. P. Royall and H. Tanaka, *Phys. Rev. Lett.*, 2010, **104**, 165702.
10 L. Porcar, P. Falus, W.-R. Chen, A. Faraone, E. Fratini, K. Hong, P. Baglioni and Y. Liu, *J. Phys. Chem. Lett.*, 2010, **1**, 126–129.
11 F. Cardinaux, E. Zaccarelli, A. Stradner, S. Bucciarelli, B. Farago, S. U. Egelhaaf, F. Sciortino and P. Schurtenberger, *J. Phys. Chem. B*, 2011, **115**, 7227–7237.
12 P. Falus, L. Porcar, E. Fratini, W.-R. Chen, A. Faraone, K. Hong, P. Baglioni and Y. Liu, *J. Phys.: Condens. Matter*, 2012, **24**, 064114.
13 E. J. Yearley, P. D. Godfrin, T. Perevozchikova, H. Zhang, P. Falus, L. Porcar, M. Nagao, J. Curtis, P. Gawande, R. Taing, I. E. Zarraga, N. J. Wagner and Y. Liu, *Biophys. J.*, 2014, **106**, 1763–1770.
14 P. D. Godfrin, I. E. Zarraga, J. Zarzar, L. Porcar, P. Falus, N. J. Wagner and Y. Liu, *J. Phys. Chem. B*, 2016, **120**, 278–291.
15 P. D. Godfrin, S. D. Hudson, K. Hong, L. Porcar, P. Falus, N. J. Wagner and Y. Liu, *Phys. Rev. Lett.*, 2015, **115**, 228302.
16 J. Riest and G. Nägele, *Soft Matter*, 2015, **11**, 9273–9280.
17 J. Riest, T. Eckert, W. Richtering and G. Nägele, *Soft Matter*, 2015, **11**, 2821–2843.
18 S. Das, J. Riest, R. G. Winkler, G. Gompper, K. G. Dhont and G. Nagele, *Soft Matter*, 2018, **14**, 92–103.
19 J. Riest, G. Nagele, Y. Liu, N. J. Wagner and P. D. Godfrin, *J. Chem. Phys.*, 2018, **148**, 065101.

20 P. Ramírez-González and M. Medina-Noyola, *Phys. Rev. E: Stat., Nonlinear, Soft Matter Phys.*, 2010, **82**, 1–15.
21 T. R. Kirkpatrick, *Phys. Rev. A: At., Mol., Opt. Phys.*, 1985, **31**, 939.
22 P. D. Godfrin, N. E. Valadez-Pérez, R. Castañeda-Priego, N. J. Wagner and Y. Liu, *Soft Matter*, 2014, **10**, 5061.
23 S. R. Kline, *J. Appl. Crystallogr.*, 2006, **39**, 895–900.
24 K. Gekko and H. Noguchi, *J. Phys. Chem.*, 1979, **83**, 2706.
25 J. M. Kim, R. Castañeda-Priego, Y. Liu and N. J. Wagner, *J. Chem. Phys.*, 2011, **134**, 064904.
26 L. Belloni, *J. Phys.: Condens. Matter*, 2000, **12**, R549.
27 Y. Liu, *Phys. Rev. E*, 2017, **95**, 020501.
28 W. van Megen, T. Mortensen, S. Williams and J. Müller, *Phys. Rev. E: Stat. Phys., Plasmas, Fluids, Relat. Interdiscip. Top.*, 1998, **58**, 6073–6085.
29 M. P. Allen and D. J. Tildesley, *Computer Simulation of Liquids*, Oxford University Press, 1987.
30 P. D. Godfrin, R. Castañeda-Priego, Y. Liu and N. J. Wagner, *J. Chem. Phys.*, 2013, **139**, 154904.
31 N. A. Seaton and E. D. Glandt, *J. Chem. Phys.*, 1987, **86**, 4668.
32 Y. Liu, W.-R. Chen and S.-H. Chen, *J. Chem. Phys.*, 2005, **122**, 044507.
33 S.-H. Chen, M. Broccio, Y. Liu, E. Fratini and P. Baglioni, *J. Appl. Crystallogr.*, 2007, **40**, s321–s326.
34 J. Bergenholtz and M. Fuchs, *Phys. Rev. E: Stat. Phys., Plasmas, Fluids, Relat. Interdiscip. Top.*, 1999, **59**, 5706–5715.
35 N. E. Valadez-Pérez, R. Castañeda-Priego and Y. Liu, *RSC Adv.*, 2013, **3**, 25110.
36 R. A. Lionberger and W. B. Russel, *J. Rheol.*, 1994, **38**, 1885.
37 A. P. R. Eberle, N. J. Wagner and R. Castañeda-Priego, *Phys. Rev. Lett.*, 2011, **106**, 105704.
38 N. E. Valadez-Pérez, Y. Liu, A. P. R. Eberle, N. J. Wagner and R. Castañeda-Priego, *Phys. Rev. E: Stat., Nonlinear, Soft Matter Phys.*, 2013, **88**, 060302(R).
39 I. Saika-Voivod, E. Zaccarelli, F. Sciortino, S. V. Buldyrev and P. Tartaglia, *Phys. Rev. E: Stat., Nonlinear, Soft Matter Phys.*, 2004, **70**, 041401.
40 W. B. Russel, N. J. Wagner and J. Mewis, *J. Rheol.*, 2013, **57**, 1555.
41 H. Lowen, T. Palberg and R. Simon, *Phys. Rev. Lett.*, 1993, **70**, 1557–1560.
42 E. Zaccarelli and W. C. K. Poon, *Proc. Natl. Acad. Sci. U. S. A.*, 2009, **106**, 15203.
43 C. P. Royall, S. R. Williams, T. Ohtsuka and H. Tanaka, *Nat. Mater.*, 2008, **7**, 556–561.
44 H. Tanaka, T. Kawasaki, H. Shintani and K. Watanabe, *Nat. Mater.*, 2010, **9**, 324–331.
45 A. M. Puertas, M. Fuchs and M. E. Cates, *J. Chem. Phys.*, 2004, **121**, 2813.
46 C. Mayer, F. Sciortino, P. Tartaglia and E. Zaccarelli, *J. Phys.: Condens. Matter*, 2010, **22**, 104110.
47 E. Zaccarelli, *J. Phys.: Condens. Matter*, 2007, **19**, 323101.

This journal is © The Royal Society of Chemistry 2018